ELSEVIER

Contents lists available at ScienceDirect

Biochemistry and Biophysics Reports

journal homepage: www.elsevier.com/locate/bbrep



Comparison of in vitro and in vivo oligomeric states of a wild type and mutant trimeric inner membrane multidrug transporter



Zhaoshuai Wang^a, Wei Lu^a, Prasangi Rajapaksha^a, Thomas Wilkop^b, Yuguang Cai^{a,*}, Yinan Wei^{a,**}

ARTICLE INFO

Keywords: FRET FRAP Disulfide trapping Membrane protein oligomer Cell membrane AcrB diffusion coefficient

ABSTRACT

Many membrane proteins exist and function as oligomers or protein complexes. Routine analytical methods involve extraction and solubilization of the proteins with detergents, which could disturb their actual oligomeric state. AcrB is a trimeric inner membrane multidrug transporter in E. coli. In previous studies, we created a mutant AcrBp223G, which behaves like a monomer when extracted from the cell membrane. However, the actual oligomeric state of AcrB_{P223G} in cell membranes remained unclear, which complicated the interpretation of the mechanism by which the mutation affects function. Here we used several complementary methods to determine the oligomeric state of $AcrB_{P223G}$ in *E. coli* cell membranes. Two sets of quantitative fluorescent techniques were exploited. For these, we created fluorescent tagged AcrB, AcrB-CFP and AcrB-YPet. Fluorescence resonance energy transfer (FRET) and fluorescence recovery after photobleaching (FRAP) were employed to characterize independently the efficiency of energy transfer between co-expressed AcrB-CFP and AcrB-YPet, and the diffusion coefficient of AcrB-YPet and AcrB_{P223G}-YPet in live E. coli cells. Second, we introduced Cys pairs at the intersubunit interface and used controlled oxidation to probe inter-subunit distances. The results from all studies converge on the conclusion that AcrB_{P223G} exists as a trimer in cell membranes, which dissociates during the purification steps. The small change in trimer affinity and structure leads to a significant loss of AcrB activity. In addition, throughout this study we developed protocols and established benchmark values, useful for further studies on membrane protein associations in cell membranes.

1. Introduction

The triplex AcrAB-TolC is one of the most well-studied multidrug efflux system in Gram-negative bacteria [1–3]. It contains an inner membrane transporter AcrB, an outer membrane channel TolC, and a periplasmic adaptor protein AcrA. Together they form a continuous structure that spans both layers of the cell membrane and the periplasmic space between the membranes. AcrAB-TolC plays an important role in conferring drug-resistance against a large array of structurally different compounds including most antimicrobials on the market [4,5]. Therefore, it has been the subject of intense studies over the past three decades. The structure of *E. coli* AcrB was first determined in 2002 [6]. Over the next 16 years close to 30 crystal structures of the protein, including wild type, mutants, or with/without bound substrate, have been deposited into the protein data bank. AcrB exists and functions as a trimer. In previous studies we have shown that the trimer stability is

critical for activity, as mutations introduced at the inter-subunit interface lead to trimer dissociation and loss of efflux activity [7]. However, the trimer stability was accessed using detergent solubilized and purified samples. It remained unclear how the mutant behaved in the cell membrane under naturel conditions. Do they predominantly exist as monomers as observed after extraction, or as trimers, or in equilibration between trimers and monomers?

A challenge in all studies on membrane protein complex and oligomerization is the potential artifact from membrane extraction and detergent solubilization. When removed from its native environment of the lipid bilayer cell membrane, loosely associated oligomers may dissociate and lead to false negative conclusions about protein interactions and their oligomeric states. Few techniques are compatible with the study of protein structure and interaction in cell membranes. Among those that are compatible, fluorescence microscopy affords many convenient quantitative opportunities [8,9]. Fluorescent tagged proteins

^a Department of Chemistry, University of Kentucky, Lexington, KY 40506, United States

^b Light Microscopy Core, University of Kentucky, Lexington, KY 40536, United States

^{*} Correspondence to: University of Kentucky, 305 Chemistry-Physics Building, Lexington, KY 40506, United States.

^{**} Correspondence to: University of Kentucky, 161B Jacob Science Building, Lexington, KY 40506, United States. E-mail addresses: Yuguang.cai@uky.edu (Y. Cai), yinan.wei@uky.edu (Y. Wei).

can be readily identified and detected in intact cells, without the need for extraction and purification. Several methods have been developed and adapted to study membrane proteins in cell membranes, including FRET and FRAP. FRET can reveal information about the distances between a donor fluorophore tagged protein and an acceptor fluorophore tagged protein [10-13]. From the level of energy transfer, the distance between acceptor and donor fluorophores and hence interaction and assembly of membrane protein complexes can be identified. FRAP measurements can reveal the diffusion kinetics and diffusion coefficients of fluorescent-tagged proteins in fluidic cell membranes [14,15]. Upon protein complexes formation, diffusion coefficients are reduced. An alternative method to probe the formation of protein complexes in cells is chemical crosslinking. Covalent linkage can be established between subunits in a protein complex in cells prior to protein extraction and purification. Bifunctional crosslinkers with different arm lengths can be employed when the structures of the proteins are unknown. When molecular structures are known, cysteine pairs can be introduced at strategic sites to investigate the distribution of monomer vs. oligomer and examine the effect of mutations on complex formation/population distribution. This method is especially useful for prokaryotic proteins, which normally contain very few intrinsic cysteine residues [16].

Here we used a combination of FRET and FRAP, as well as a controlled disulfide trapping method, to investigate the oligomeric state of $AcrB_{P223G}$ in the cell membrane. We found that the mutant existed predominantly as trimers in the cell membrane, in contrast to its detergent solubilized state. We have also discovered that the dissociation of $AcrB_{P223G}$ trimer during extraction and purification is due to the high detergent concentration necessary for efficient extraction. Removal of excess detergent during purification promoted re-association of $AcrB_{P223G}$ trimers.

2. Materials and methods

2.1. Cloning, protein expression and purification

The gene CFP or YPet was inserted at the C-terminus of AcrB in plasmids pBAD33-AcrB or pBAD18-AcrB, respectively, to create pBAD33-AcrB-CFP or pBAD18-AcrB-Ypet. A short 5 residue linker, GGSGG, was also included in between the C-terminus of AcrB and the N-terminus of the fluorescent tag. Plasmids pBAD33-AcrB_{P223G}-CFP or pBAD18-AcrB_{P223G}-Ypet were created by site directed mutagenesis using the corresponding plasmids as templates. DNA sequence encoding the protein of interest was confirmed via sequencing.

Plasmids encoding the indicated AcrB constructs were transformed into the *E. coli* strain $MG1655\Delta acrB$ for expression. A single colony was picked from the LB agar plate and used to inoculate 3 mL LB culture containing the appropriate antibiotics (chloramphenicol for pBAD33 constructs and ampicillin for pBAD18 constructs). The cultures were grown overnight and then used to inoculate 1 L of fresh LB-antibiotics media. The cultures were incubated at 37 °C until the OD600 reached 1.0. Arabinose was added to a final concentration of 0.2% to induce protein expression and the cultures were grown at 28 °C for 15 h. Bacteria cells were then harvested and stored at -80 °C before purification. The protein was purified as described elsewhere [7, 17, 18].

2.2. Preparation of the microscopy samples

E. coli strain *MG1655*Δ*acrB*, transformed with the indicated plasmid, was cultured in LB media containing the appropriate antibiotic overnight. The next morning, the overnight culture was diluted 20 fold into fresh media and cultured to an OD600 of \sim 0.5. Protein expression was under basal condition without induction. The cell culture was directly dropped onto a pre-made agar gel pad to prepare samples for microscopy, similar to earlier described protocols [19]. To prepare the gel pad, 25 mL of 1% of agarose in LB media was autoclaved, and then cooled to \sim 50 °C. 70 μL of the solution was pipetted into a Gene Frame

(ThermoFisher Scientific) mounted at the center of a glass slide. A cover film was immediately applied on top of the gel. The gel pad could be stored at 4 $^{\circ}C$ in a sealed container for several weeks. To prepare the microscopy sample, the slide was first warmed to room temperature. The cover slide was removed and 2 μL of *E. coli* culture was applied onto the gel surface. By slightly tilting the gel pad back and forth several times, the *E. coli* suspension was evenly spread over the gel pad surface. After 5 min of drying, the gel pad was removed from the gel pad frame with tweezers and remounted on a fresh glass slide with the *E. coli* covered surface facing up and covered using a 0.17 mm thick cover glass.

2.3. Scanning laser confocal microscope imaging

All imaging and measurement of *E. coli* cells expressing fluorescent proteins were conducted using the Zeiss LSM 880 with Airyscan laser scanning confocal microscope using a Plan-Apochromat $63 \times /1.4$ NA oil immersion objective.

For the donor photobleaching FRET (pbFRET) method, we used the Airyscan detector in super resolution mode. The detector gain was set at 800 and the donor (AcrB-CFP) fluorescence was monitored between 465 and 505 nm. During the imaging and photobleaching process, the Ar laser was used as the light source at full power. The 458 nm line of the Ar laser was used as the excitation source for AcrB-CFP imaging and photobleaching. The 514 nm line of the Ar laser was used to bleach AcrB-YPet.

For the spectrum-based FRET method, a photomultiplier detector and a variable stepwise emission dispersion was used to obtain fluorescence emission spectra of the donor-only sample (*E. coli* expressing AcrB-CFP), the acceptor-only sample (*E. coli* expressing AcrB-YPet), and the FRET sample (*E. coli* expressing both AcrB-CFP and AcrB-YPet). The gain of the PMT detector was set at 800. The spectrum resolution was 5 nm.

The diffusion coefficient of AcrB-YPet in the *E. coli* membrane was measured at the single cell level using FRAP. The *E. coli* cells were imaged using the 514 nm laser as the excitation source at 1% of the full output power. The corresponding fluorescence signal was detected through a bandpass filter of 525–700 nm using the Airyscan detector in super resolution mode with the gain set at 800. Photobleaching was conducted using the 514 nm laser at full power. All measurements were conducted within 2 h of the deposition of *e. coli* cells on the gel pads at $21\,^{\circ}$ C. More details about the data analysis and calculation are described in Cai et al. [20]

2.4. Blue-native PAGE (BN-PAGE)

BN-PAGE was conducted as described in detail with minor modifications [21]. Briefly, purified AcrB samples were mixed with blue native loading buffer at a final concentration of 0.5 M 6-aminohexanoic acid, 5% Coomassie blue G-250, 5% glycerol, pH 7.0, and loaded to a 4–20% gradient polyacrylamide gel (BIO-RAD, Hercules, CA). Electrophoresis was performed using the cathode buffer (50 mM tricine, 7.5 mM imidazoole, 0.02% Coomassie brilliant blue G-250, pH 7.0) and anode buffer (25 mM imidazole, pH 7.0) at 15 mA, in a 4 $^{\circ}$ C refrigerator for 2–4 h. The protein bands were finally visualized with Coomassie Blue staining and de-staining.

2.5. Drug susceptibility assay

AcrB activity was usually determined by a drug susceptibility assay. The MIC of different strains were measured as described [22]. Briefly, an acrB deficient $E.\ coli$ strain $(BW25113\Delta acrB)$ was used as the host cell. The $BW25113\Delta acrB$ strain transformed with plasmid-encoded WT AcrB or pQE70 vector were used as positive and negative controls, respectively. Plasmids encoding different AcrB mutants were transformed into $BW25113\Delta acrB$ as well. Freshly transformed cells were plated on

LB-agarose plates containing 100 μ g/mL ampicillin and 50 μ g/mL kanamycin. The same ampicillin and kanamycin concentrations were used throughout the study. A single colony was inoculated into a LB medium supplemented with ampicillin and kanamycin. The exponential-phase cultures of different strains were diluted to an OD600nm of 0.1 with LB broth. 10 μ L of this diluted culture was used to inoculate 1 mL LB medium containing the indicated concentration of erythromycin or novobiocin. The cultures were incubated under shaking at 37 °C for 6 h. Absorbance at 600 nm of each culture was measured to determine the minimum inhibitory concentration (MIC). This activity assay was conducted under the basal AcrB expression condition. Each experiment was repeated a minimum of three times.

2.6. Kinetic studies of AcrB association

Purified $AcrB_{P223G}$ -CFP and $AcrB_{P223G}$ -YPet freshly eluted from the Ni-NTA column were mixed at a 1:1 molar ratio, and the increase of the FRET emission (ex/em at 430/530 nm, respectively) was monitored over time

2.7. In vivo Cu(Phen)3 oxidation

Crosslinking of the Cys pair at the intersubunit interface was conducted as described with minor modifications [23]. Briefly, cell cultures (5 mL) expressing the indicated AcrB constructs were grown to an OD600 of $\sim\!1.2$, and then centrifuged, washed twice with 5 mL of phosphate buffer (50 mM NaPi, 100 mM NaCl, pH7.5), and finally resuspended in 200 μL phosphate buffer. Stock solution of 150 mM CuSO4 was prepared in water. Phen (170 mM) was dissolved in 70% ethanol. For 200 μL of sample, 2 μL CuSO4 solution was mixed with 6 μL of Phen solution and immediately added to the mixture. The samples were incubated on ice for 10 or 20 min as indicated, before a stop solution was added (20 mM Tris, 8 mM NaH2PO4, pH 7.8, 12.5 mM EDTA). Samples were centrifuged to remove the supernatant, and the cell pellets were processed and subjected to anti-AcrB immunoblotting analysis as described [24].

3. Results

3.1. AcrB-CFP and AcrB-YPet are active

Introduction of a fluorescence protein at the C-terminus of inner membrane proteins has been used in several studies as a tool to probe the topology and localization of proteins of interest. We do not expect the tag to affect the structure and activity of AcrB. Activities of AcrB and the fluorescent fusion proteins were examined using the MIC assay (Table 1). Two AcrB substrates were used in the assay, novobiocin and erythromycin. For both substrates, AcrB fusion proteins are largely active, indicating that the tagged proteins form native-like trimer structures. The two fold decrease of MIC of erythromycin for AcrB-Ypet could be due to reduced expression level of the protein or mild effect of the tag on function-related conformational changes of AcrB.

3.2. FRET efficiency in CFP/YPet tagged AcrB and AcrB $_{P223G}$

Two independent FRET methods were used to determine the apparent energy transfer efficiency of co-expressed AcrB-CFP/AcrB-YPet,

Table 1 MIC (μ g/mL) of $BW25113\Delta acrB$ containing plasmids encoding indicated AcrB constructs.

Plasmid	AcrB	AcrB-CFP	AcrB-YPet	/
Novobiocin	320	320	320	20
Erythromycin	160	160	80	20

and $AcrB_{P223G}$ -CFP/ $AcrB_{P223G}$ -YPet. Since AcrB form trimers, the protein population will be a diverse combination of trimers containing one donor and two acceptor subunits, or one acceptor and two donor subunits, as well as FRET-silent trimers containing only donor or acceptor subunits. Since the goal is to qualitatively compare the efficiency between the WT and P223G AcrB, we determined the apparent FRET efficiency (E) of the two constructs.

The first method is pbFRET [8,25]. The pbFRET measures the fluorescence decay of the donor emission in the presence and absence of the acceptor when the donor is undergoing photobleaching. During photobleaching, the fluorescence intensity of the donor is recorded as a function of time. The recorded data is plotted and fitted according to an exponential decay in order to obtain the decay constant τ :

$$I = I_0 + Ae^{-\frac{t}{\tau}} \tag{1}$$

The donor's fluorescence decay rate $(1/\tau)$ is proportional to the photobleaching rate, which is in turn proportional to the number of molecules in the excited singlet state. A higher FRET efficiency corresponds to a slower photobleaching rate and a larger decay constant τ . The FRET efficiency can be expressed as functions of the donor fluorescence intensity decay constant of the donor-acceptor pair τ_D^{DA} and the donor only sample τ_D^{D} :

$$E = 1 - \frac{\tau_D^D}{\tau_D^{DA}} \tag{2}$$

 au_D^D and au_D^{DA} are decay constants, au is obtained from the fitting the fluorescent intensity curves over time for donor emission, from the donor only sample and donor-acceptor pair, respectively [25].

The intensity decay curves were obtained from two photobleaching time-lapse image sequences, collected before and after acceptor photobleaching, which were corrected for background. Detailed experimental and calculation procedure can be found in the Supplementary material. In Fig. 1, representative images and extracted fluorescence decay curves are shown. As shown in Figs. 1b and 1d, the photobleaching process destructed a large portion of the acceptor molecules (YPet), which abolished the corresponding FRET, and thus the fluorescence signal of the donor (CFP) for both AcrB-CFP and AcrB_{P223G}-CFP increased. Furthermore, after the photobleaching of the acceptor, the CFP fluorescence decayed faster during the imaging process, as reflected by the decrease of decay constant τ in both the wild type and the mutant proteins. The observed increase in CFP fluorescence intensity and the decrease in τ indicated the existence of FRET both in the wild type and the mutant proteins. The FRET efficiency is calculated to be $50 \pm 6\%$, and $22 \pm 3\%$ for wild type and P223G AcrB, respectively, from measurements of multiple cells as listed in Table 2.

The second method is the spectrum-based FRET. The Zeiss confocal microscope is equipped with a spectral dispersion mechanism that can be used to obtain an emission spectrum of each pixel in a fluorescent image. This capacity enabled us to measure the spectrum-based FRET efficiency, which is based on the analysis of corrected spectra curve integrals [13,26]. The spectrum-based FRET method has several advantages over the simpler conventional acceptor photobleaching methods [26]. Among the main advantages are that it monitors simultaneous changes in donor and acceptor fluorescence, and accounts through correction factors for crosstalk. Therefore, it is a more robust and reliable method.

We imaged *E. coli* cells expressing AcrB-CFP, AcrB-YPet, or both, as well as their P223G counterpart using the spectral emission finger-printing. According to the spectrum-based FRET definition, the FRET efficiency E is calculated as [9,26]:

$$E = \frac{I_{\lambda D}^A \cdot Q^D / Q^A}{I_{\lambda D}^D + I_{\lambda D}^A \cdot Q^D / Q^A}$$
(3)

where $I_{\lambda D}^{A}$ is the acceptor sensitized fluorescence intensity, $I_{\lambda D}^{D}$ is the donor fluorescence emission intensity directly excited at donor

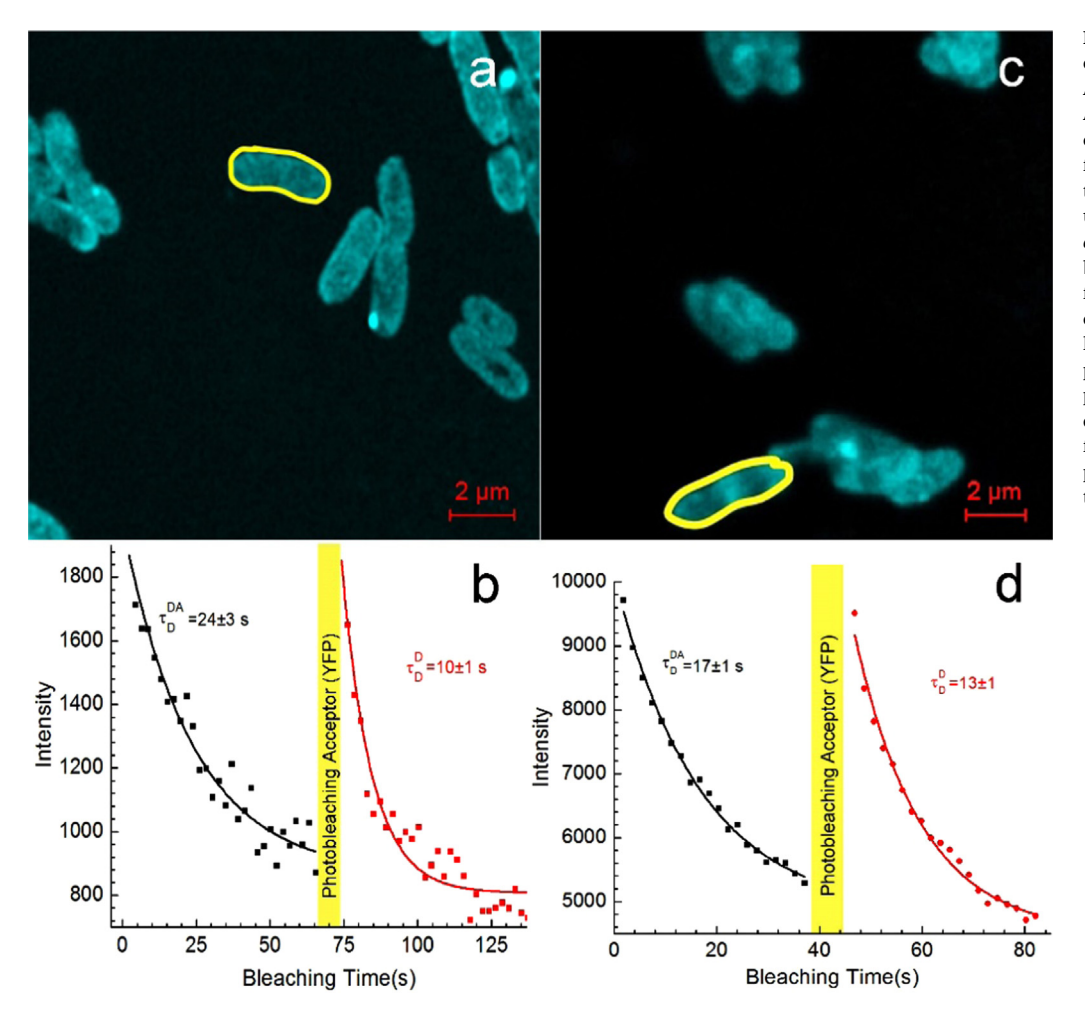


Fig. 1. The photobleaching of E. coli cells expressing both AcrB-CFP and AcrB-YPet, or AcrB_{P223G}-CFP and AcrB_{P223G}-Ypet. Representative images of wild type (a.) and P223G (c.) The fluorescence images were recorded in the CFP emission band (465-505 nm), under 458 nm laser excitation. The E. coli cells used for analysis are marked by the yellow outline and their mean fluorescence intensities of this Region of Interest (ROI) in a sequence of timelapse images are extracted (black data points in b and d) before and after the photobleaching of the acceptor (red data points in b and d). The fit of fluorescence intensity decay curves is plotted in b (WT) and d (P223G) for these two representative E. coli cells.

 Table 2

 The FRET efficiency of CFP and YPet labeled AcrB in E. coli cells.

FRET efficiency	pbFRET method	Number of measurements	spectrum method	Number of measurements
WT	50 ± 6%	20	35 ± 6%	16
P223G	22 ± 3%	12	26 ± 5%	30

wavelength obtained from the donor pure spectra, Q^D/Q^A is the ratio of donor to acceptor quantum yield. The quantum yield of CFP and YPet are 0.40 and 0.77 respectively [27,28]. I_{AD}^A and I_{AD}^D were obtained through measurements from C and F channels (Fig. 2) after corrections. Detailed calculation can be found in the Supplementary material. The FRET efficiency values calculated based on the spectrum FRET method is shown in Table 2.

Two FRET methods were used to determine the energy transfer efficiency to validate the accuracy of the obtained values. According to the spectrum method, the FRET efficiency values between the WT and

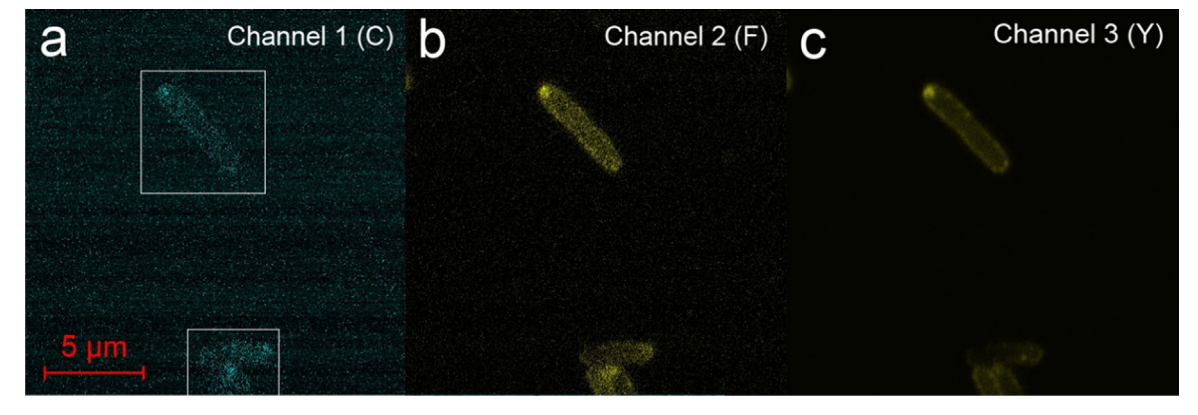


Fig. 2. Representative images collected from the Airyscan detector. a) The fluorescence image in Channel 1 (*C*, CFP), which recorded fluorescence signal excited at 458 nm collected between 473 and 483 nm and b) The fluorescence image in Channel 2 (F, FRET), which recorded fluorescence signal excited at 458 nm and collected over 523–533 nm band. c) The fluorescence image in Channel 3 (Y, YPet), recorded the fluorescence excited at 514 nm over 523–533 nm. Region of interests were highlighted in white boxes.

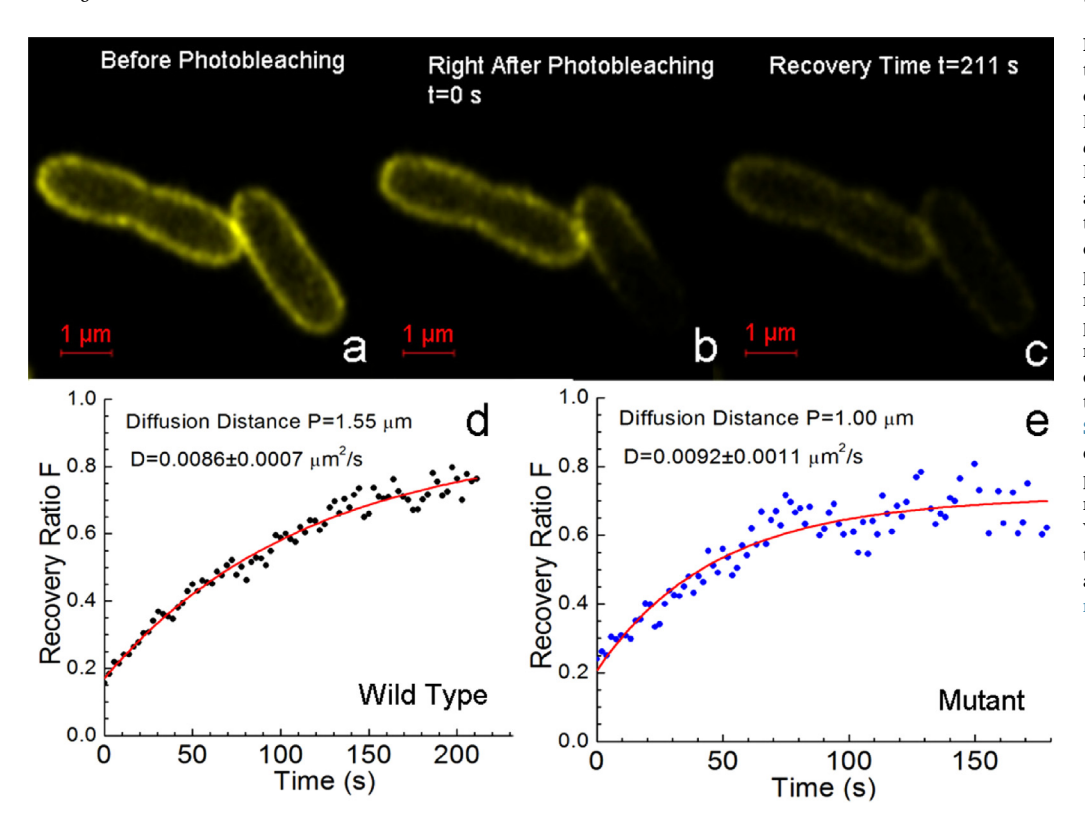


Fig. 3. FRAP measurement for the determination of the diffusion coefficient of AcrB-YPet in E. coli cell membranes. Representative image of wild type E. coli cells expressing AcrB-YPet. b. Image of the E. coli cells immediately after the bottom half of the E. coli on the right was photobleached. c. Image of the same E. coli cells 211s after photobleaching. d. The fluorescence recovery ratio of the bleached area plotted as a function of recovery time measured for AcrB-YPet. The diffusion coefficient was obtained from fitting the recovery curve as described in the Supplementary material. e. The fluorescence recovery ratio of bleached area plotted as a function of recovery time measured for the mutant AcrB_{P223G}-YPet. The diffusion coefficient was obtained from fitting the recovery curve as described in the Supplementary material.

P223G AcrB are not significantly different, while there are significant differences for the pbFRET method obtained values. This difference reflects the variation between cells sampled during the experiment, as well as discrepancies in data collection and analysis of the two methods. For both methods, significant energy transfer was detected for $AcrB_{P223G}$ fluorescent fusion proteins, suggesting that at least a large portion of $AcrB_{P223G}$ still exists as oligomers (most likely trimers) in the cell membrane.

3.3. Comparison of diffusion coefficients determined using the FRAP technique

The FRAP method was used to measure the diffusion coefficient of AcrB-YPet and AcrB_{P223G}-YPet in the E. coli cell membrane. The rationale of this experiment is based on the correlation of diffusion rate with the molecular weight of proteins. Larger proteins, or protein complexes tend to diffuse slower, and thus trimeric AcrB should diffuse substantially slower than monomeric AcrB. If AcrB_{P223G} exists predominantly as monomers in the cell membrane, it should have a much larger diffusion coefficient than that of WT AcrB. Fig. 3 illustrates representative images of E. coli cells expressing AcrB-YPet before and after photobleaching. Before photobleaching (Fig. 3a), clear yellow envelopes can be observed around each E. coli cells. The bottom half of the cell on the right was then photobleached. Immediately after bleaching, the region is completely dark (Fig. 3b). After 211 s of recovery, weak but significant fluorescent contours could be identified due to diffusion of AcrB-YPet from unaffected area to the bleached area. Because of continuous imaging during the recovery period, the overall image intensity is reduced. Fluorescence of an unaffected area was also collected in parallel $(I_{cntl}(t))$ and used for correction of the ongoing photobleaching during imaging. Recovery of fluorescence intensity $(I_{bl}(t))$ over time after photobleaching was paired with the control intensity to calculate the Recovery Ratio F:

$$F(t) = \frac{I_{bl}(t)}{I_{cntl}(t)} \tag{4}$$

Fitting of the plot of F(t) over time revealed the diffusion coefficients of AcrB-YPet and AcrB_{P223G}-YPet to be 0.0086 \pm 0.0007 and 0.0092 \pm 0.0011 μ m²/s, respectively. Details on the calculations are presented in the Supplementary material [11].

While in Fig. 3 we observed clear membrane localization, in Figs. 1 and 2 the observation was not as clear. The major difference between the experimental conditions in obtaining Fig. 3 (clear membrane localization) and Figs. 1 and 2 (not as clear) was the excitation wavelength and protein expression level. Fig. 3 was obtained using the 514 nm laser as the excitation source. In contrast, Figs. 1 and 2 were obtained using the 458 nm laser as the excitation source. Both Figs. 1 and 2 are studies of the FRET effect, which measures the energy transfer from the donor CFP to the acceptor YPet after CFP was excited. The CFP signal is intrinsically weak, as a result, higher excitation intensity needs to be used. In addition, the observation window is close to the excitation wavelength, which led to a higher level of non-specific background fluorescence. In contrast, Fig. 3 was obtained using the 514 nm excitation, and observed in the range of 525-700 nm. In addition, YPet intrinsically has stronger emission, thus a lower excitation intensity was used. This combination reduced the level of non-specific background fluorescence signal. In terms of protein expression, Figs. 1 and 2 were obtained using E. coli cells expressing both AcrB-CFP and AcrB-YPet, while Fig. 3 was obtained using cells only expressing AcrB-YPet. The coexpression condition reduced the expression level of each individual construct, which also contributed to the higher background and less clear membrane localization in Figs. 1 and 2.

3.4. Optimization of the reaction condition for the disulfide trapping method

Fluorescent imaging of membrane proteins in live cells is challenging and potentially impacted by artifacts [29,30]. We used additional biophysical methods to confirm the observations from our microscopy studies. First we conducted disulfide trapping. For our purpose, we need to identify an experimental condition in which disulfide bonds do not form between AcrB subunits in a trimer during cell growth, thus the protein expression and assembly would not be affected by the formation

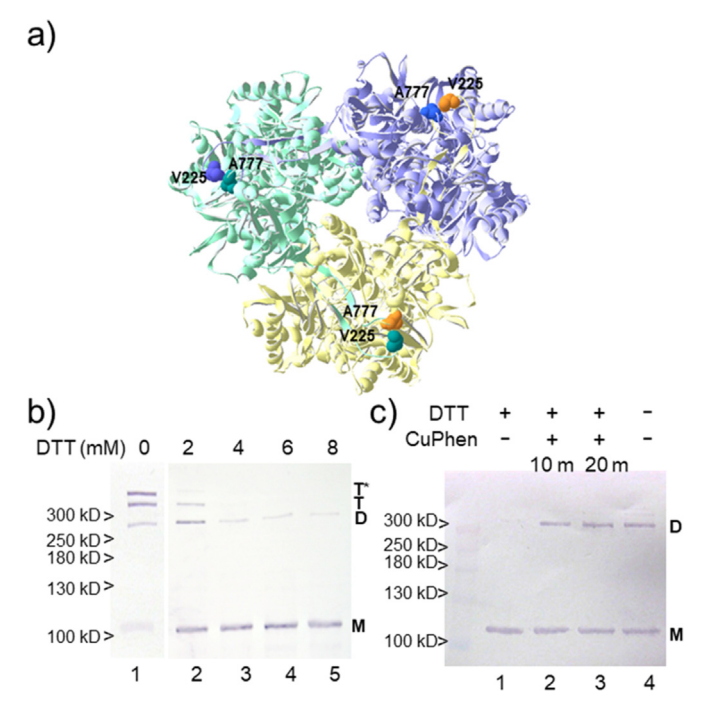


Fig. 4. Inter-subunit disulfide bond formation in AcrB trimer. a) Head view (from the periplasmic side) of an AcrB trimer. The side chains of V225 and A777 were highlighted using a space fill model. Residues are colored according to their corresponding subunit. b) The spontaneous formation of disulfide bonds in $AcrB_{V225C/A777C}$ could be prevented by the addition of DTT in the medium. Lane 1 reveals three high molecular weight bands, which are dimer and two trimer bands (linear and circular) [24]. Most high molecular weight bands disappeared in the presence of 4 mM DTT. c) The co-expression of $AcrB_{V225C}$ and $AcrB_{A777C}$ leads to the formation of inter-subunit disulfide bonds in a hybrid trimer, which migrated as a mixture of monomer and dimers in non-reducing SDS-PAGE (lane 4). When cultured in the presence of DTT, no disulfide bonds formed (lane 1). Oxidation by $Cu(Phen)_3$ for 10 or 20 min on ice lead to the formation of disulfide bonds.

of disulfide bonds. Then the proteins are quickly oxidized before detection to promote disulfide bond formation, which locks oligomers via covalent bond and prevents them from dissociating during the subsequent detergent extraction and purification steps. Toward these goals, we used several AcrB mutants created in previous studies. AcrB contains two intrinsic Cys residues, which were replaced with Ala to construct a Cys-less AcrB. Later mutations were introduced into this Cysless background. As shown in Fig. 4A, AcrB forms a tight trimer. V225 and A777 are located at the interface in the periplasm between neighboring subunits, which form disulfide bond when both are mutated into Cys under normal culturing conditions [31]. The formation of a disulfide bond between Cys225 and Cys777 in the double mutant AcrB_{V225C/A777C} is close to 100% and does not affect its efflux activity. We have previously shown that when $AcrB_{V225C}$ and $AcrB_{A777C}$ were coexpressed, disulfide bonds formed in mixed trimers containing both subunits and the resultant protein sample migrated as a mixture of monomer and disulfide bond-linked dimers [24]. Using these constructs as tools, we first examined under what condition the disulfide bond ceased to form during protein expression.

We cultured the *E. coli* strain $BW25113\Delta acrB$ transformed with a plasmid encoding $AcrB_{V225C/A777C}$. Protein expression was examined under basal condition without induction. Under normal culturing condition in LB medium without DTT, disulfide bonds formed between C225 and C777 as expected, and $AcrB_{V225C/A777C}$ migrated mainly as a covalently linked trimer with a small portion migrating as dimers (Fig. 4B, lane 1). As previously described, we speculate that the two bands T and T* correspond to a linear trimer (three subunits linked by two disulfide bonds between A–B, and B–C) and a circular trimer (with

an additional disulfide bond connecting C–A) [24]. To prevent the formation of the disulfide bond, DTT was included in the LB medium at concentrations of 2, 4, 6 and 8 mM. DTT at concentrations higher than 5 mM noticeably slowed down cell growth. At 4 mM, the spontaneous formation of disulfide bonds was largely inhibited. The majority of proteins migrated as monomers, with $\sim\!10\%$ migrating as a dimer band. An additional increase of DTT did not further reduce the amount of dimers. Therefore, we choose to add 4 mM DTT in the media while culturing the cells.

Next, we co-expressed AcrB_{V225C} and AcrB_{A777C} to monitor the formation of disulfide bonds upon oxidation. To compare the efficiency of spontaneous disulfide bond formation and disulfide bonds formed upon addition of Cu(Phen)₃, BW25113∆acrB transformed with plasmid encoded AcrB_{V225C} and AcrB_{A777C} was cultured in the presence or absence of 4 mM DTT overnight. Next, cell culture grown in the presence of DTT was centrifuged and washed twice using an ice cold phosphate buffer (50 mM NaPi, 200 mM NaCl, pH 7.5) buffer. Cell pellet was then resuspended in the same phosphate buffer, and Cu(Phen)3 was added as described in Materials and Methods. The mixture was incubated on ice for 10 or 20 min, and then the cells were processed and analyzed using anti-AcrB Western blot. As shown in Fig. 4C, a dimer band was present when the cells were cultured in normal LB medium, but was absent when the culture was grown in the presence of DTT. Incubation of cells grown in the presence of DTT with Cu(Phen)3 effectively converted a portion of protein into dimers, at a similar level as in the culture grown in the absence of Cu(Phen)3. A short treatment of 10 min on ice has been proven to be effective and was used in the rest of the study.

3.5. $AcrB_{P223G}$ exists as trimers in cell membrane

We have previously reported that when cultured under normal conditions in LB, in the absence of reducing agent, AcrB_{P223G/V225C/} A777C spontaneously forms trimers, which partially restores the efflux activity of the protein due to the P223 to Gly mutation [7]. Here the cells were cultured in the presence of 4 mM DTT and then oxidized quickly using Cu(Phen)3 on ice for 10 min. As shown in Fig. 5A, $AcrB_{P223G/V225C/A777C}$ formed disulfide bonded trimers. When $\beta\text{-mer}$ captoethanol was added to the loading dye, the majority of the higher molecular weight species was reduced and migrated as monomers. We found that AcrB in SDS-loading dye could not be boiled. This heat treatment routinely used to fully denature and unfold proteins leads to AcrB precipitation. Thus we speculate that the residual amount of dimer band upon reduction is due to incomplete protein reduction/denaturation. Result from this new oxidation experiment is consistent with the result from spontaneous disulfide bond formation experiments. Thus we conclude that while the P223G mutation reduced trimer affinity, the mutant protein still exists predominantly as trimer in cell membranes. The dissociation into monomers likely occurred during membrane extraction, in which the large excess of detergent molecules disrupts protein-protein interaction.

If this is indeed the reason for the observed monomeric P223G after purification, then reducing the detergent concentration should lead to protein re-association into trimers. During protein purification, 2% (w/ v) DDM was used for membrane extraction. Extracted solution was incubated with Ni-NTA resin for 2 h, and then beads were collected in a column and washed using a wash buffer containing 0.03% (w/v) DDM. The wash step took approximately 10 min. At this step reassociation could not occur either even though the detergent concentration was lowered, since proteins were immobilized to resins via their C-terminal histag. Association of monomers into trimers could occur as soon as the proteins were freed from the resin using an elusion buffer containing 0.03% (w/v) DDM. The elution process took a few minutes. We noticed that when freshly eluted AcrB_{P223G} was analyzed immediately using BN-PAGE, AcrB_{P223G} migrated largely as monomers, with a very small portion migrated as timers [7]. However, when we analyzed the sample after overnight incubation, the majority of the monomers re-associated

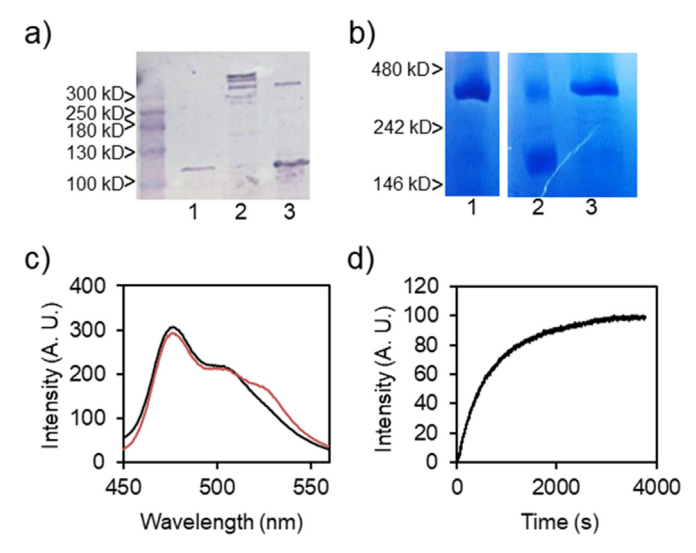


Fig. 5. Trimerization of AcrB_{P223G}. a) Anti-AcrB Western blot analysis. AcrB_{P223G/V225C/R777C} cultured in the presence of 4 mM DTT did not form disulfide bonds (lane 1). Oxidation using Cu(Phen)₃ for 10 min on ice led to the formation of oligomer bands (lane 2). Upon reduction, most of the oligomer bands except for part of the dimer band were reduced to monomers (lane 3). b) Freshly purified wild type AcrB migrated as trimers in BN-PAGE analysis (lane 1), while freshly purified AcrB_{P223G} migrated as monomers (lane 2). After overnight incubation, AcrB_{P223G} also forms trimers (lane 3). c) Fluorescence emission spectra (ex 430 nm) of AcrB_{P223G}-CFP and AcrB_{P223G}-YPET mixed at 1:1 molar ratio. The black trace was collected right after incubation, while the red trace was collected after 3 h. The shoulder peak with apparent wavelength of ~525 nm is the FRET emission. d) Increase of FRET fluorescence (ex/em at 430/530 nm, respectively) over time.

into trimers (Fig. 5b, lane 3). To examine the time scale of assembly, we took advantage of the fluorescent fusion proteins $AcrB_{P223G}$ -CFP and $AcrB_{P223G}$ -YPet. When freshly purified, both were mainly monomers as revealed by BN-PAGE (not shown). When mixed together, a clear FRET signal (ex/em wavelengths of 430/530 nm, respectively) increased over time, indicating that oligomerization occurred quickly and a significant portion of monomers associated into dimers and then trimers within hours (Fig. 5c, d). This result indicated that $AcrB_{P223G}$ is capable of trimerization, supporting our hypothesis that the protein exists as trimers, rather than monomers, in the cell membrane under the native condition.

4. Discussion

To effectively compete with lipids and solubilize membrane proteins, detergent needs to be added at high concentrations. In our routine protocol, as well as many published protocols involving membrane protein purification, concentration of 1–2% (w/v) is normally used. For membrane proteins, the effective protein concentration is defined by its molar ratio to detergent concentration, since the number of detergent micelles defines the actual "space" that the protein can occupy. Thus, a higher detergent concentration correlates to a lower protein concentration, which promotes oligomer dissociation. As an estimation, the surface area of an E. coli cell is approximately 6 μM². Assuming 50% of the cell surface is occupied by lipid, and an average lipid surface area of 50 Å², the number of lipid molecules per cell is 6×10^6 [32]. Under our over-expressing condition, there are ~3200 AcrB trimers, or 10,000 AcrB subunits per E. coli cell [24], thus the molar ratio (molarity of protein over molarity of lipid) is 10,000: 6×10^6 , or 1: 600. The actual number of "free" lipids per AcrB subunit is much less, considering there are other membrane proteins that also need to be surrounded and "solubilized" by lipids. During membrane extraction, if 2% (w/v) DDM is used, the molar concentration is ~0.04 M. We routinely resuspend

cell pellet from 1 L culture overexpressing AcrB in 40 mL buffer during detergent extraction, which roughly correlated to 4 mg of AcrB $(3.2 \times 10^{-8} \text{ mol})$ per 40 mL of buffer containing 2% DDM $(1.6 \times 10^{-3}$ mol), thus the molar ratio is 1:50,000. This ratio is close to \sim 1% of the original concentration. In the case of fluorescent tagged AcrB, the expression level is about five to ten-fold less. But the molar ratio change during detergent extraction is similar. This is a very rough estimation without considering the contribution of lipids and other membrane proteins from the cells that also bind to each other and to detergent molecules during the membrane solubilization/extraction process. But the dilution effect due to the need to add extra detergents is apparent. While tightly bound oligomers such as wild type AcrB could survive short term exposure to a high detergent concentration during membrane extraction, weaker membrane protein oligomers such as AcrB_{P223G} dissociate during the process. Thus, it is important to characterize the oligomeric stage and complex formation of membrane proteins in cell membranes.

With the fast development of hardware and software, fluorescence microscopy is keeping on pushing boundaries in life science research. Fluorescence microscopy is uniquely useful in studying protein-protein interaction and localization since they can be used to analyze live cells, thus can probe target proteins under the more natural or physiological condition. In this study, we used three different methods, bpFRET, spectrum FRET, and FRAP. Obtaining reliable FRET efficiency of a target protein complex in intact cells is challenging, complicated by noises and factors such as protein expression level and population variation. This intrinsic variation is also highlighted by our observation that the FRET efficiency values determined using the two FRET methods are different for the same sample. However, both methods revealed significant FRET in the fluorescent tagged AcrB_{P223G} mutant, indicating oligomers exist. This result is confirmed using the FRAP measurement, as the diffusion coefficients for the WT and P223G AcrB-YPet fusion proteins are not statistically different, indicating that the proteins are similar in size.

Additional evidence supporting the trimeric state of AcrB_{P223G} comes from disulfide trapping experiment. When using the disulfide trapping method to probe protein-protein interaction, we need to keep in mind that formation of a covalent bond may serve as an energy sink to drive the thermodynamic equilibrium toward the associated state. DeGrado and co-workers has recognized this problem and modified the disulfide trapping method to incubate the protein with a GSH/GSSG mixture [33,34]. The GSH/GSSG mixture provides a buffered redox condition to allow the proteins to adjust and better represent their oligomeric state. Here we aimed at determining the natural oligomeric state of membrane proteins in the cell membrane. We found that by adding 4 mM DTT in the LB media, spontaneous disulfide bond formation in AcrB was greatly reduced. Thus we were able to introduce a pair of Cys at the inter-subunit interface and use it to probe protein oligomerization, while only inducing disulfide bond to form after cells are collected and right before they are lysed for analysis. By doing so, we avoided potential bias that could come from the energy sink of disulfide bond formation during cell growth. We acknowledge that the experimental design is based on the assumption that trimer dissociation in cell membrane is a slow process compared to the time necessary to remove DTT and initiate oxidation. This is consistent with a report by Bowie and co-workers, who discovered that membrane proteins could have very high kinetic stabilities [35].

5. Conclusions

In summary, we used three orthogonal methods to assess the oligomeric state of an AcrB mutant, P223G. Results from all three methods are consistent with the hypothesis that $AcrB_{P223G}$ exists predominantly as trimers in cell membranes. The high concentration of detergent necessary for membrane extraction could lead to dissociation of membrane protein complexes, which in turn lead to false negative

conclusions about loosely associated complexes and oligomers.

Acknowledgement

We thank the UK Light Microscopy Core for the usage of the Zeiss LSM 880 microscope and technical support. We thank Dr. Chris Richards for valuable discussions. This study is supported by NSF grant CHE-1709381 (YW).

Appendix A. Transparency document

Supplementary data associated with this article can be found in the online version at doi:10.1016/j.bbrep.2018.10.006.

References

- Z. Wang, G. Fan, C.F. Hryc, J.N. Blaza, I.I. Serysheva, M.F. Schmid, W. Chiu, B.F. Luisi, D. Du, An allosteric transport mechanism for the AcrAB-TolC multidrug efflux pump, Elife 6 (2017).
- [2] X.Z. Li, P. Plesiat, H. Nikaido, The challenge of efflux-mediated antibiotic resistance in Gram-negative bacteria, Clin. Microbiol. Rev. 28 (2015) 337–418.
- [3] H. Nikaido, Y. Takatsuka, Mechanisms of RND multidrug efflux pumps, Biochim. Biophys. Acta 1794 (2009) 769–781.
- [4] H. Venter, R. Mowla, T. Ohene-Agyei, S. Ma, RND-type drug efflux pumps from Gram-negative bacteria: molecular mechanism and inhibition, Front. Microbiol. 6 (2015) 377.
- [5] P. Ruggerone, S. Murakami, K.M. Pos, A.V. Vargiu, RND efflux pumps: structural information translated into function and inhibition mechanisms, Curr. Top. Med. Chem. 13 (2013) 3079–3100.
- [6] S. Murakami, R. Nakashima, E. Yamashita, A. Yamaguchi, Crystal structure of bacterial multidrug efflux transporter AcrB, Nature 419 (2002) 587.
- [7] L. Yu, W. Lu, Y. Wei, AcrB trimer stability and efflux activity, insight from Mutagenesis studies, PLOS One 6 (2011) e28390.
- [8] T.M. Jovin, D.J. Arndt-Jovin, Luminescence digital imaging microscopy, Annu. Rev. Biophys. Biophys. Chem. 18 (1989) 271–308.
- [9] J.R. Lakowicz, Principles of Fluorescence Spectroscopy, Kluwer Academic, Plenum, NY, 1983.
- [10] L. Chen, L. Novicky, M. Merzlyakov, T. Hristov, K. Hristova, Measuring the energetics of membrane protein dimerization in mammalian membranes, J. Am. Chem. Soc. 132 (2010) 3628–3635.
- [11] L. Scott, S. Zelenin, S. Malmersjo, J.M. Kowalewski, E.Z. Markus, A.C. Nairn, P. Greengard, H. Brismar, A. Aperia, Allosteric changes of the NMDA receptor trap diffusible dopamine 1 receptors in spines, Proc. Natl. Acad. Sci. USA 103 (2006) 762–767.
- [12] N. Del Piccolo, K. Hristova, Quantifying the interaction between EGFR Dimers and Grb2 in live cells, Biophys. J. 113 (2017) 1353–1364.
- [13] H.J. Chial, P. Lenart, Y.Q. Chen, APPL proteins FRET at the BAR: direct observation of APPL1 and APPL2 BAR domain-mediated interactions on cell membranes using FRET microscopy, PLoS One 5 (2010) e12471.
- [14] S.M. van den Wildenberg, Y.J. Bollen, E.J. Peterman, How to quantify protein diffusion in the bacterial membrane, Biopolymers 95 (2011) 312–321.

- [15] G. Rayan, J.E. Guet, N. Taulier, F. Pincet, W. Urbach, Recent applications of fluorescence recovery after photobleaching (FRAP) to membrane bio-macromolecules, Sensors 10 (2010) 5927–5948.
- [16] G. Pascal, C. Medigue, A. Danchin, Persistent biases in the amino acid composition of prokaryotic proteins, Bioessays 28 (2006) 726–738.
- [17] L. Yu, W. Lu, C. Ye, Z. Wang, M. Zhong, Q. Chai, M. Sheetz, Y. Wei, Role of a conserved residue R780 in Escherichia coli multidrug transporter AcrB, Biochemistry 52 (2013) 6790–6796.
- [18] W. Lu, M. Zhong, Y. Wei, Folding of AcrB subunit precedes trimerization, J. Mol. Biol. 411 (2011) 264–274.
- [19] A.L. Bottomley, L. Turnbull, C.B. Whitchurch, E.J. Harry, Immobilization techniques of bacteria for live super-resolution imaging using structured illumination microscopy, Methods Mol. Biol. 1535 (2017) 197–209.
- [20] Y. Cai, T. Wilkop, Y. Wei, Data on spectrum-based fluorescence resonance energy transfer measurement of *E. coli* multidrug transporter AcrB, Data Brief (2018).
- [21] I. Wittig, H.P. Braun, H. Schagger, Blue native PAGE, Nat. Protoc. 1 (2006) 418-428
- [22] Y. Takatsuka, H. Nikaido, Threonine-978 in the transmembrane segment of the multidrug efflux pump AcrB of Escherichia coli is crucial for drug transport as a probable component of the proton relay network, J. Bacteriol. 188 (2006) 7284-7289.
- [23] A.G. Hughson, G.F. Lee, G.L. Hazelbauer, Analysis of protein structure in intact cells: crosslinking in vivo between introduced cysteines in the transmembrane domain of a bacterial chemoreceptor, Protein Sci. 6 (1997) 315–322.
- [24] W. Lu, Q. Chai, M. Zhong, L. Yu, J. Fang, T. Wang, H. Li, H. Zhu, Y. Wei, Assembling of AcrB trimer in cell membrane, J. Mol. Biol. 423 (2012) 123–134.
- [25] J. Szollosi, D.R. Alexander, The application of fluorescence resonance energy transfer to the investigation of phosphatases, Methods Enzymol. 366 (2003) 203–224.
- [26] D. Megias, R. Marrero, B. Martinez Del Peso, M.A. Garcia, J.J. Bravo-Cordero, A. Garcia-Grande, A. Santos, M.C. Montoya, Novel lambda FRET spectral confocal microscopy imaging method, Microsc. Res. Tech. 72 (2009) 1–11.
- [27] G. Patterson, R.N. Day, D. Piston, Fluorescent protein spectra, J. Cell Sci. 114 (2001) 837–838.
- [28] A.W. Nguyen, P.S. Daugherty, Evolutionary optimization of fluorescent proteins for intracellular FRET, Nat. Biotechnol. 23 (2005) 355–360.
- [29] C. King, V. Raicu, K. Hristova, Understanding the FRET signatures of nteracting membrane proteins, J. Biol. Chem. 292 (2017) 5291–5310.
- [30] C. King, S. Sarabipour, P. Byrne, D.J. Leahy, K. Hristova, The FRET signatures of noninteracting proteins in membranes: simulations and experiments, Biophys. J. 106 (2014) 1309–1317.
- [31] M.A. Seeger, C. von Ballmoos, T. Eicher, L. Brandstatter, F. Verrey, K. Diederichs, K.M. Pos, Engineered disulfide bonds support the functional rotation mechanism of multidrug efflux pump AcrB, Nat. Struct. Mol. Biol. 15 (2008) 199–205.
- [32] T.H. Bayburt, S.G. Sligar, Membrane protein assembly into nanodiscs, FEBS Lett. 584 (2010) 1721–1727.
- [33] L. Cristian, J.D. Lear, W.F. DeGrado, Determination of membrane protein stability via thermodynamic coupling of folding to thiol-disulfide interchange, Protein Sci. 12 (2003) 1732–1740.
- [34] L. Cristian, J.D. Lear, W.F. DeGrado, Use of thiol-disulfide equilibria to measure the energetics of assembly of transmembrane helices in phospholipid bilayers, Proc. Natl. Acad. Sci. USA 100 (2003) 14772–14777.
- [35] R.E. Jefferson, T.M. Blois, J.U. Bowie, Membrane proteins can have high kinetic stability, J. Am. Chem. Soc. 135 (2013) 15183–15190.